Engineering 4 (2018) 398–405

Contents lists available at ScienceDirect

Engineering

journal homepage: www.elsevier.com/locate/eng

Research
Green Industrial Processes—Article

Mechanochemical-Assisted Leaching of Lamp Phosphors: A Green Engineering Approach for Rare-Earth Recovery

Steff Van Loy [a], Koen Binnemans [b], Tom Van Gerven [a,*]

[a] Department of Chemical Engineering, KU Leuven, Heverlee B-3001, Belgium
[b] Department of Chemistry, KU Leuven, Heverlee B-3001, Belgium

ARTICLE INFO

Article history:
Received 4 December 2017
Revised 14 March 2018
Accepted 17 May 2018
Available online 22 May 2018

Keywords:
Mechanochemistry
Rare-earth elements
Lamp phosphor waste
Ball-milling
Solvometallurgy

ABSTRACT

Rare-earth elements (REEs) are essential metals for the design and development of sustainable energy applications. Recycling these elements from waste streams enriched in them is crucial for securing an independent future supply for sustainable applications. This study compares the mechanisms of mechanical activation prior to a hydrometallurgical acid-leaching process and a solvometallurgical mechanochemical leaching process for the recovery of REEs from green lamp phosphor, $LaPO_4$:Ce^{3+}, Tb^{3+}. After 60 min of processing time, the REE leaching rates showed a significant enhancement of 60% after cycled mechanical activation, and 98% after the combined mechanochemical leaching process. High-resolution transmission electron microscopy (HR-TEM) imaging disclosed the cause for the improved REE leaching rates: The improved leaching and leaching patterns could be attributed to changes in the crystal morphology from monocrystalline to polycrystalline. Reduction of the crystallite size to the nanoscale in a polycrystalline material creates irregular packing of chemical units, resulting in an increase in defect-rich grain boundaries in the crystals, which enhances the leaching process. A solvometallurgical method was developed to combine the mechanical activation and leaching process into a single step, which is beneficial for operational cost. This results in an efficient and simple process that provides an alternative and greener recycling route for lamp phosphor waste.

1. Introduction

Rare-earth elements (REEs) are essential metals for the design and development of sustainable energy-related applications such as renewable energy technologies (e.g., solar, wind, and thermoelectric converters), lighting, and magnetic materials [1,2]. Recycling critical REEs from end-of-life consumer goods (e.g., permanent magnets, lamp phosphors, and Ni-metal hydride (MH) batteries) and recovering these elements from industrial residues (e.g., bauxite residue and phosphogypsum) are the most prominent pathways to ensure an independent supply for future applications, aside from primary mining [3–5]. Recycling has major advantages over primary supply, including a smaller environmental footprint, shorter lead times, and cheaper sources of material [6]. Moreover, recycling may provide a solution for the over-supply of "unwanted" REEs, and it can contribute to a steady supply of the more critical REEs (neodymium (Nd), dysprosium (Dy), and terbium (Tb)), thus mitigating the so-called "balance problem" [7].

Several studies have been conducted on recycling REEs from waste, with a particular focus on permanent magnets and lamp phosphors [4,8–14]. Phosphors in compact fluorescent lamps (CFLs) are a rich source of one of the most critical and highly valued elements, Tb, which is retained in the green phosphor ($LaPO_4$:Ce^{3+}, Tb^{3+} or $CeMgAl_{11}O_{19}$:Tb^{3+}) [15]. Hydrometallurgy is a traditionally established and easy method for the recovery of valuable metals. $LaPO_4$:Ce^{3+},Tb^{3+} can be dissolved using hot concentrated sulfuric acid (H_2SO_4) at temperatures ranging from 120 to 230 °C [16]. Pyrometallurgical methods that apply strongly alkaline conditions (35 wt% NaOH, 150 °C) in an autoclave or that involve the presence of molten alkali (e.g., Na_2CO_3 at 1000 °C or $Ba(OH)_2$ at 950 °C) are used to transform rare-earth phosphates into oxides, which can be leached under mild conditions [4,13,14,16,17]. However, the use of an alkali flux leads to the formation of silicates, due to the presence of fine glass particles, which impede downstream separation of REE. Recently, researchers reported the use of fungi for the bioleaching of rare-earth phosphates (i.e., monazite) as a possible green alternative procedure [18].

The recycling of rare-earth phosphates or aluminates requires high amounts of energy and harsh chemical conditions. Therefore,

* Corresponding author.
E-mail address: tom.vangerven@kuleuven.be (T. Van Gerven).

https://doi.org/10.1016/j.eng.2018.05.015

the use of mechanical stresses to enhance (leaching) reactions has been postulated as a green alternative reaction route. This nonconventional reaction route, commonly named mechanochemistry (MC), has gained the attention of several researchers for the recovery of critical metals. MC techniques were successfully applied to Li-ion batteries, tungsten carbide tool waste, indium tin oxide (ITO) glass, and lamp phosphor waste [19,20]. A mechanochemical method can enhance both the leaching yield and the leaching rate of barely soluble metals from end-of-life materials or industrial waste streams.

In our previous study, it was proven that mechanical activation (MA) by grinding as a pretreatment step prior to leaching is a valuable method for improving the recovery of REEs from lanthanum phosphate (LAP) lamp phosphor waste [21]. It was postulated that this pretreatment introduces defects into the crystal lattice, resulting in a disordered crystal structure that extensively accelerates the subsequent leaching operation, thus avoiding the need for thermal activation. However, if the high-energy milling (i.e., the MA) is physically and temporally separated from the leaching process, not all introduced excitation states (effects) are used to their full extent (Fig. 1) [22]. Since some defects are not stable and have short relaxation times, highly excited activation states decay before the leaching stage is initiated [22,23]. Therefore, a process of MA followed by leaching only utilizes the long-lived excitation states. Using a combined milling-leaching (mechanochemical) process, all excitation states can be used, including the short-lived states. The activated outer shell of the particle can be simultaneously leached, thereby exposing fresh surface and improving the leaching performance.

In this study, two activation-leaching procedures are studied for the recovery of REEs from LAP lamp phosphor. MA and subsequent chemical leaching are applied during the first procedure to determine the effect of the milling and leaching time and to propose an optimal cyclic milling/leaching procedure. The effect of the milling operation on the crystal structure is determined using high-resolution transmission electron microscopy (HR-TEM). With the second procedure, MA is combined with the leaching operation (mechanochemical leaching) in a single step and compared with the previous activation-leaching procedure, in order to provide more insight into the importance of short- and long-lived states, and the advantages of a mechanochemical recycling process.

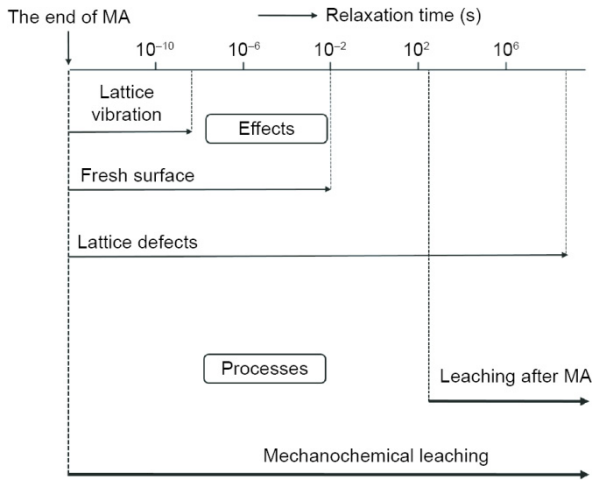

Fig. 1. A generalized graph with duration and relaxation time of different excitation states (effects) after termination of MA. The leaching processes show the distinction between the involved excitation states (effects). (Adapted from Ref. [22])

2. Experimental process

2.1. Chemicals

LAP lamp phosphor ($LaPO_4$:Ce^{3+},Tb^{3+}) at 99% purity was kindly provided by OSRAM (Munich, Germany). Acidic solutions were prepared using ultrapure water (18.2 MΩ·cm^{-1} at 25 °C; Sartorius Arium pro, Göttingen, Germany), concentrated sulfuric acid (H_2SO_4, 95%–97%; Sigma-Aldrich, Diegem, Belgium), and concentrated methanesulfonic acid (MSA) (CH_3SO_3H, 99.5%; Sigma-Aldrich, Diegem, Belgium). The rare-earth salts ($La_2(SO_4)_3$, 99.9%; $Ce_2(SO_4)_3{\cdot}8H_2O$, 99.9%; $Tb_2(SO_4)_3{\cdot}8H_2O$, 99.9%) were purchased from Sigma-Aldrich (Diegem, Belgium). $Ce(SO_4)_2{\cdot}4H_2O$ (99%) was bought from Acros Organics (Geel, Belgium). The inductively coupled plasma (ICP) standards (Fluka, 1000 mg·L^{-1}) were purchased from Sigma-Aldrich (Diegem, Belgium).

2.2. Instrumentation

Quantitative analysis of the leachates was performed by ICP-optical emission spectrometry (ICP-OES) (Optima 8300; PerkinElmer, USA) or by ICP-mass spectrometry (ICP-MS) (Elan 9000; PerkinElmer, USA) for concentrations lower than 10 μg·L^{-1}. The concentrations of REEs in the LAP lamp phosphor were determined by quantitative analysis of the solutions (in triplicate) after the sample was fully digested in an aqua regia solution via microwave-assisted digestion (Speedwave Xpert; Berghof Products + Instruments, Eningen, Germany). The particle-size distribution of the activated samples was characterized using a laser particle-size analyzer (Mastersizer 3000; Malvern Panalytical, Malvern, UK) using the laser diffraction method in liquid mode. X-ray powder diffraction (XRD) data were recorded using an X-ray powder diffractometer (D2 Phaser; Bruker, Karlsruhe, Germany). Concentrations of Ce(IV) were determined by an ultraviolet-visible (UV-Vis) spectroscopy device (Lambda 365; PerkinElmer, USA) using 10 mm quartz vials.

The powder crystal defects and morphology were investigated using HR-TEM. The powder sample was deposited on carbon tape, and a layer of 20 nm of carbon was deposited using a carbon coater. A Helios Nanolab 650 dual beam scanning electron microscope (SEM)/focused ion beam (FIB) system (FEI, Eindhoven, the Netherlands) was used to prepare lamellar cross-sections on the particles in several steps, starting with the deposition of a 2 μm thick platinum (Pt) layer (2 μm × 12 μm) using ion-beam Pt deposition. Final thinning was performed with an FIB energy of 2 kV and a current of 23 pA.

Bright-field TEM (BF-TEM) images and selected-area electron diffraction (SAED) patterns were performed using an FEI Tecnai G2 electron microscope (FEI, Eindhoven, the Netherlands) operated at 200 kV. High-angle annular dark-field scanning TEM (HAADF-STEM) and energy-dispersive X-ray (EDX) spectroscopy mapping were performed on an FEI Tecnai Osiris electron microscope (FEI, Eindhoven, the Netherlands) operated at 200 kV.

2.3. Activation/leaching procedure

The activation of the phosphor powder was conducted using a planetary ball-mill (Pulverisette 7 premium; Fritsch, Idar-Oberstein, Germany) in air. Phosphor samples were mixed with zirconia balls (ϕ = 1 mm) with a ball-to-powder (B:P) ratio of 50:1 (by weight), and then placed in a zirconia bowl (80 mL inner volume). The activation of the phosphors consisted of two modes: (dry) MA and (wet) mechanochemical activation. During the first mode, the dry sample was milled for various time periods (15–60 min). Subsequently, the activated sample was mixed with

a 2 mol·L^{-1} H_2SO_4 solution with a liquid-to-solid (L:S) ratio of 20 mL·g^{-1} and shaken for 15 min (200 r·min^{-1}). During the second mode, the sample was mixed with concentrated H_2SO_4 or MSA at a varying L:S ratio (1.0–3.0 mL·g^{-1}) and activated for different time periods (15–60 min). The wetted powder was mixed with ultrapure water to a final solution with an L:S ratio of 20 mL·g^{-1}. A cycled MA mode was employed in which samples were sequentially milled for 15 min followed by 15 min of leaching in 2 mol·L^{-1} H_2SO_4, in order to compare with the mechanochemical leaching (15 min of simultaneous milling and leaching). The effect of the presence of liquid upon grinding was determined by performing a cycled milling procedure (15 min) on the powder in the presence of ethylene glycol, followed by a leaching step (15 min). Ethylene glycol was chosen because of its similar viscosity to H_2SO_4. During all activation procedures, the rotational speed was fixed at 600 r·min^{-1} and intermediate cooling periods (10 min) were used for each 15 min of milling time to avoid accumulated heat.

2.4. Measurements

2.4.1. Leaching yield of REE in leachate

The leaching yield (%) was calculated by Eq. (1):

$$\text{Leaching yield} = \frac{\text{Amount of metal in the leachate}}{\text{Total amount of metal in the sample}} \times 100\% \quad (1)$$

The expressed leaching yield represents the average yield of the individual REEs in the phosphor, as leaching percentages are similar for all REEs (lanthanum (La), cerium (Ce), and Tb).

2.4.2. Oxidation of cerium ions

Measurements of the concentrations of Ce(III) and Ce(IV) for the oxidation experiments were obtained using UV-Vis absorption spectroscopy. Calibration solutions containing 2.0×10^{-5} mol·L^{-1} Ce(III), La(III), Tb(III), and Ce(IV) were prepared in 2 mol·L^{-1} H_2SO_4. The Beer-Lambert law could be applied at the characteristic maximum absorption wavelength of Ce(IV) (315 nm) obtained from spectra recorded from 200 to 600 nm, since there is no absorption overlap with other REEs at these wavelengths.

A correlation coefficient above 0.999 was obtained. The oxidation yield for Ce(IV), the so-called Y_{ox} (%), was defined as follows (Eq. (2)):

$$Y_{ox} = \frac{n_{Ce(IV)}}{n^{init}_{Ce(III)}} \times 100\% \quad (2)$$

where $n_{Ce(IV)}$ represents the number of moles of oxidized Ce(IV), which is calculated from the UV-Vis measurement, and $n^{init}_{Ce(III)}$ refers to the total initial number of moles of Ce(III) in solution after digestion, which is obtained from the ICP-OES analysis.

3. Results

3.1. Chemical leaching of mechanically activated LAP

Rare-earth phosphates (e.g., $LaPO_4$:Ce^{3+},Tb^{3+}) are difficult to dissolve due to their monoclinic lattice structure, which is similar to that of monazite ore. This structure leads to a high chemical stability and a high energy input requirement to break the chemical bonds. The crystals therefore show high resistance to acid attack. Less than 1% of REE can be leached using 2 mol·L^{-1} H_2SO_4 at room temperature (25.0 °C ± 0.5 °C) (Fig. 2). However, LAP lamp phosphor is shown to be sensitive to the effect of MA. Fig. 2 shows the REE leaching yield, 45% and 51%, respectively, from a mechanically activated sample (with activation time of 30 and 60 min, respectively) after 5 min of leaching. The effect of MA is significant,

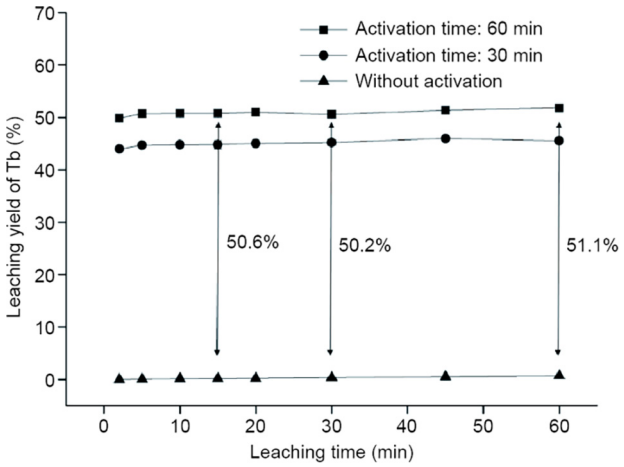

Fig. 2. Recovery of Tb from LAP in terms of leaching yield of Tb versus leaching time. Chemical leaching conditions: L:S = 20 mL·g^{-1}, 2 mol·L^{-1} H_2SO_4, T = 25 °C. MA conditions: 600 r·min^{-1}, ϕ_{ball} = 1 mm, B:P = 50:1.

amounting to a 200-fold increase in leaching yield. It can be noted that the leaching of the MA sample is a spontaneous reaction, due to the change in the dissolution mechanism, which changes, for the non-activated sample, from chemically controlled to a diffusion-controlled reaction after activation [21,24]. The milling time shows a positive effect on the leaching yield of the MA sample (Fig. 3), with a sharp increase in leaching during the first 15 min of milling. Afterward, the effect is substantially smaller, which can be explained by the change in particle size. After an initial particle-size reduction (a mean numerical size of 0.15 μm after 5 min of milling), the particles start to aggregate as an effect of the elongated milling, resulting in an increase in the mean numerical particle size, which is 0.30 μm after 15 min and 0.37 μm after 60 min.

3.2. Physicochemical changes of mechanically activated LAP

A common strategy to increase the reactivity of solids includes the introduction of physicochemical changes, such as changes in particle size, specific surface area, crystal lattice, and chemical composition. Elongated milling causes changes in the crystallite size and induces strain in the crystal lattice [21]. The mechanical

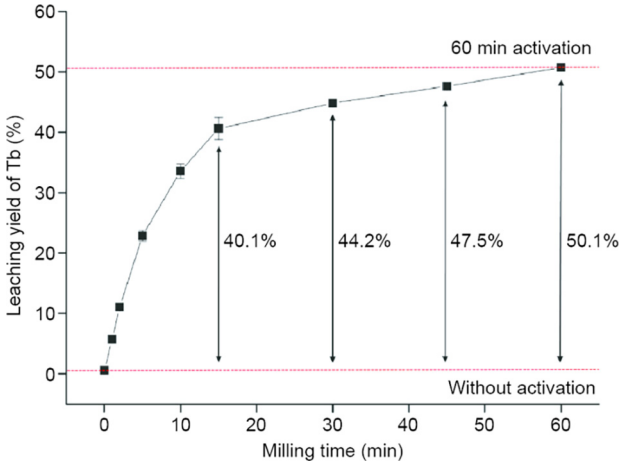

Fig. 3. Recovery of Tb from LAP in terms of leaching yield of Tb versus milling time. Chemical leaching conditions: L:S = 20 mL·g^{-1}, 2 mol·L^{-1} H_2SO_4, T = 25 °C. MA conditions: 600 r·min^{-1}, ϕ_{ball} = 1 mm, B:P = 50:1. Error bars indicate standard deviations, which are calculated based on the leaching results from three replicates. Error bars that are not visible are smaller than the symbol of the data point.

forces introduce crystal defects (e.g., point defects and dislocations), resulting in an increased (X-ray-based) amorphous content (Fig. 4). A peak shift (indicated in red) can be noted as an effect of the changes in the crystal lattice and strain. The increased amorphicity, which is derived from the decreasing peak intensity and peak broadening, was posed by various researchers as the most likely major mechanism for the improved leachability of the LAP powder [21,24–26]. Nevertheless, no conclusive results were reported for the detailed structural changes or for the localization of the amorphous phase in the MA particles, which induced enhanced leaching of the REEs.

To visualize the changes in the crystal structure, the formation of defects, and the increase in amorphous content, HR-TEM imaging was performed during different milling stages (0, 5, 15, and 60 min). The unmilled LAP powder was shown to be a strongly crystalline material characterized by a monoclinic crystal structure. The high level of crystallinity is shown in Fig. 5(a), along with the SAED pattern (Fig. 5(b)). The SAED pattern shows a well-ordered structure and thus indicates a fully monocrystalline material. The close-packed network and the chemical bonding hinder the breaking of existing chemical bonds and the formation of new chemical bonds during the leaching process.

Within the first milling stage, grinding results in a reduction of particle size. However, with extended milling, particles become more reactive, resulting in the formation of aggregates. The formation of these aggregates is observable within 5 min of milling time, as visualized in Fig. 5(c), which shows the aggregate surrounded by small grounded material. BF-TEM images and SAED patterns taken from the grains after 5 min milling time suggest that the material is mostly monocrystalline (Fig. 6(a)). No amorphization of the particles was noted at the grain edges of the particles (Fig. 6(b)). Part of the material did undergo changes toward a more polycrystalline material (Fig. 6(c)), which is indicated by the SAED pattern showing a beaded ring (Fig. 6(d)). This change from a monocrystalline material toward a polycrystalline material proceeds with increasing milling time. After 15 min of milling, the powder has transformed to an (almost) fully polycrystalline material (Fig. 7(a)). The higher magnification BF-TEM image shows the grain boundaries and nanocrystallites within the material, along with the corresponding SAED pattern (Fig. 7(b)). At this stage, still, no amorphous content was found at the edges or in the bulk of the particle. The density of the unmilled and milled samples (15 min) was, respectively, $(2.0120 \pm 0.0771)\ g{\cdot}cm^{-3}$ and $(1.8713 \pm 0.0680)\ g{\cdot}cm^{-3}$. Therefore, the measured densities are not statistically different.

The surface of the powdered sample started showing some small degree of amorphization of the surface after 60 min of milling time (Fig. 7(c)). Nevertheless, the amount of amorphous content was negligible in comparison with the remaining particle surfaces of the bulk powder (Fig. 7(d)). In the transformation from a monocrystalline to a polycrystalline material, many boundaries (grain boundaries) with coherent crystalline units (grains) are created. The irregular packing of the solid material promotes chemical reaction by enhancing the diffusion. The grain boundary, which retains high amounts of natural crystal defects (i.e., dislocations and unidimensional defects), will be part of the diffusion pathway. The changing crystal structure (from monocrystalline to polycrystalline) can therefore be associated with the improved leaching rate and yield [27]. These results show, for the first time, that the enhanced leaching that follows MA is caused by the transformation of the material's structure from monocrystalline to polycrystalline, rather than by the formation of amorphous material, as has been commonly put forth as explanatory mechanism. The largest yield rate improvement was recorded after 15 min of milling time, which corresponded to an (almost) full transformation to polycrystalline material (Fig. 3). Extending the milling time will further improve the leaching yield by reducing the crystallite size and thus creating more grain boundaries. However, the extent of the MA effect progressively decreases.

In addition to causing physical changes, high-intensity milling may induce chemical changes in the crystal lattice. In this case, the oxidation of Ce(III) to Ce(IV) under the influence of MA was studied, and a visual color change from colorless $Ce_2(SO_4)_3$ to yellowish $Ce(SO_4)_2$ was observed (Fig. 8). Munnings et al. [28] has already reported the spontaneous stress-induced oxidation of cerium ions in gadolinium (Gd)-doped ceria. The oxidation of Ce(III) showed a strong increase between 15 and 30 min of milling

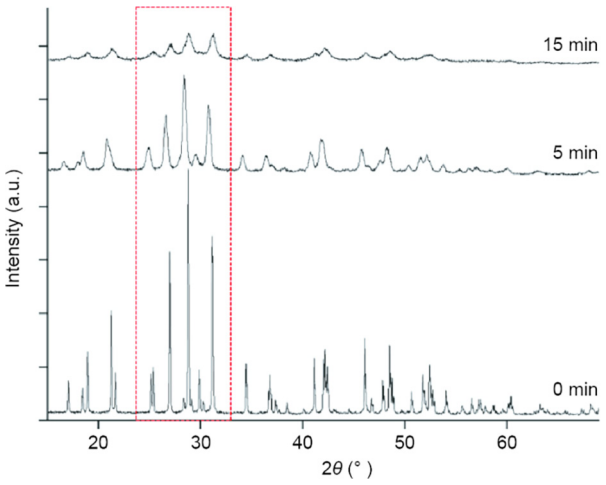

Fig. 4. Changes in the XRD pattern of the LAP lamp phosphor for different activation times (600 r·min^{-1}, ϕ_{ball} = 1 mm, B:P = 50:1).

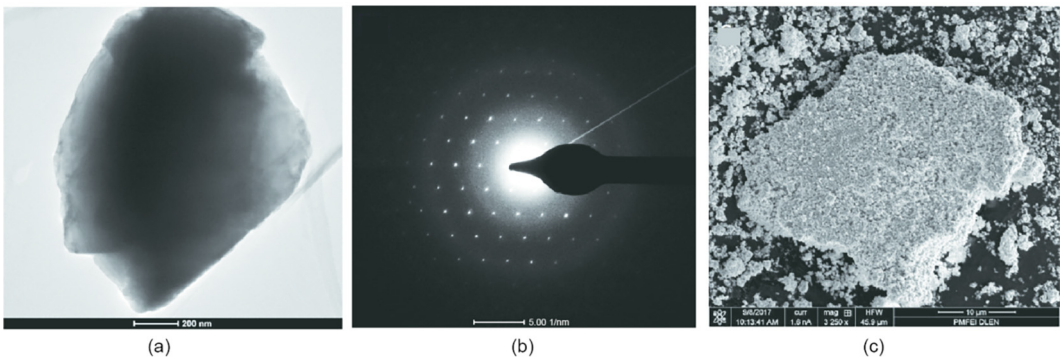

Fig. 5. (a) BF-TEM image of a particle from the unmilled LAP sample; (b) corresponding SAED pattern of unmilled LAP sample; (c) SEM image of a formed aggregate after 5 min of milling time.

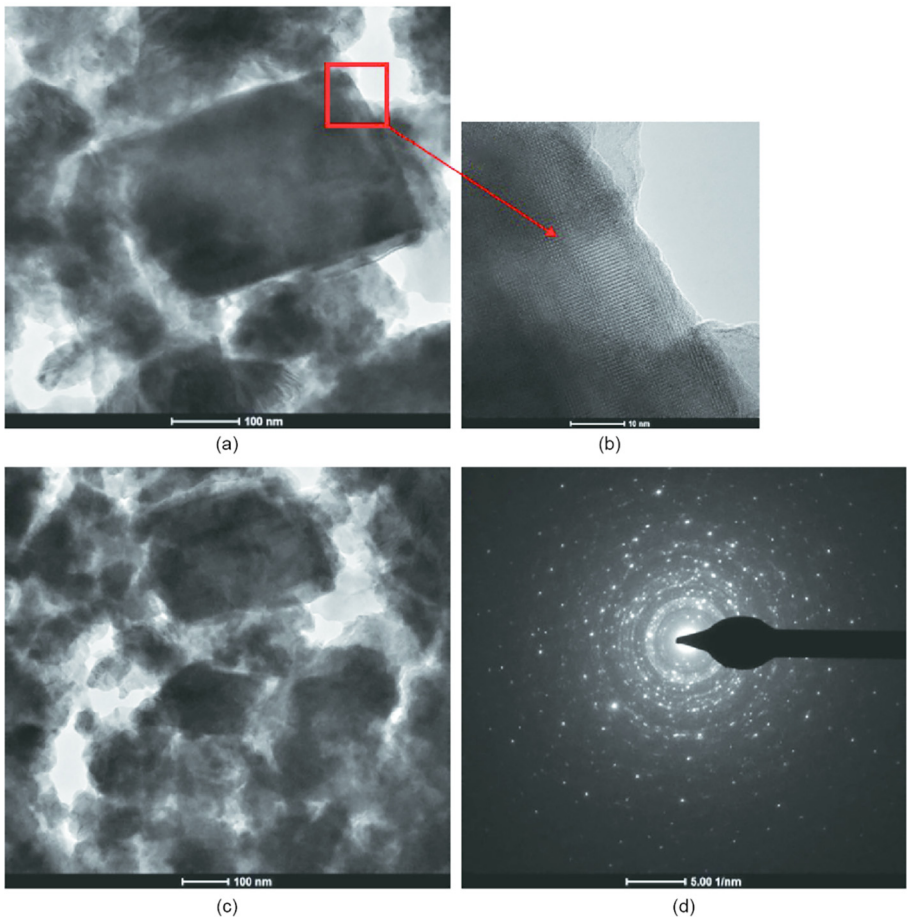

Fig. 6. (a) BF-TEM image of the grain boundary of a crystalline particle after 5 min of milling time; (b) magnification of the particle edges of a crystalline particle after 5 min of milling time; (c) BF-TEM image of the bulk powder after 5 min of milling time; (d) corresponding SAED pattern of the bulk powder after 5 min of milling time.

time, with Y_{ox} increasing from 2.2% to 14.4% (Table 1). A further increase in milling time yielded no more significant change in the Ce(IV) content. To prove the concept of stress-induced oxidation, the vessels were flushed with nitrogen gas (N_2) for 5 min, in order to remove most of the oxygen (O_2) in the atmosphere. In the flushed atmosphere, the Y_{ox} only reached 2.0% after 60 min milling time. This proves the interference of air in the vessel, with O_2 acting as an oxidizing agent. The oxidation of Ce(III) can be considered to be advantageous for the downstream separation of REEs, due to the chemical difference between REEs in the trivalent and tetravalent states [29].

3.3. Chemical and mechanochemical leaching of LAP

In order to compare the mechanochemical leaching of LAP lamp phosphor powder with its mechanically activated counterpart, separate experiments were performed. During these experiments, concentrated H_2SO_4 (boiling point of 337 °C) or concentrated MSA (boiling point of 167 °C at 10 mmHg (1 mmHg ≈ 133.322 Pa)) were selected because of their high boiling points and viscosity, as high-energy milling may result in locally high temperatures and pressures. Therefore, the choice of acid is important in order to avoid pressure buildup in the grinding vessels. Moreover, MSA is considered to be environmentally friendly [30]. Since no water was involved during this leaching process, this method can be categorized as a solvometallurgical method [31]. To determine the optimal L:S ratio, a set of experiments was conducted with varying L:S ratios, as shown in Fig. 9. Increasing the amount of liquid increased the extent of dissolution of the REEs from LAP lamp phosphor powder, with an optimum L:S of 1.5 $mL \cdot g^{-1}$. Upon further increase in the amount of liquid, the leaching yield decreased with the use of MSA. The results showed a significantly beneficial effect of H_2SO_4 on the REE leaching from LAP lamp phosphor powder, in comparison with MSA. The optimum L:S ratio can easily be explained by the damping of the mechanical impact forces at higher L:S ratios, while inefficient liquid-solid contact can be expected to occur at lower L:S ratios. The damping effect is less pronounced with the use of H_2SO_4, which could be an effect of the difference in acid viscosity. Full REE recovery was achieved using 2.5 $mL \cdot g^{-1}$ H_2SO_4, while at the optimum L:S ratio (1.5 $mL \cdot g^{-1}$), 98% of REEs were leached within 60 min of milling/leaching time.

Comparative studies were performed with mechanochemical leaching (i.e., simultaneous milling and acid leaching) and sequential leaching of both cycled mechanically activated samples and cycled wet-milled samples (i.e., simultaneous milling and wetting) (Fig. 10). The results confirmed the beneficial influence of mechanochemical leaching on the recovery of REEs from LAP lamp phosphor powder in comparison with the dry-milling procedure. Up to 73% of the REEs were recovered from the mechanochemical mode, compared with 41% from the cycled mechanical activation and 10% from the cycled wet milling, from samples that were activated for 15 min. After 60 min of milling, the leaching yield increased to 98%, 81%, and 16%, respectively, for the mechanochemical, cycled mechanically activated, and cycled wet-milled samples. The milling/leaching time reflects the total processing time, which corresponded to a sequence of 15 min milling and 15 min leaching. Dry MA had significant beneficial

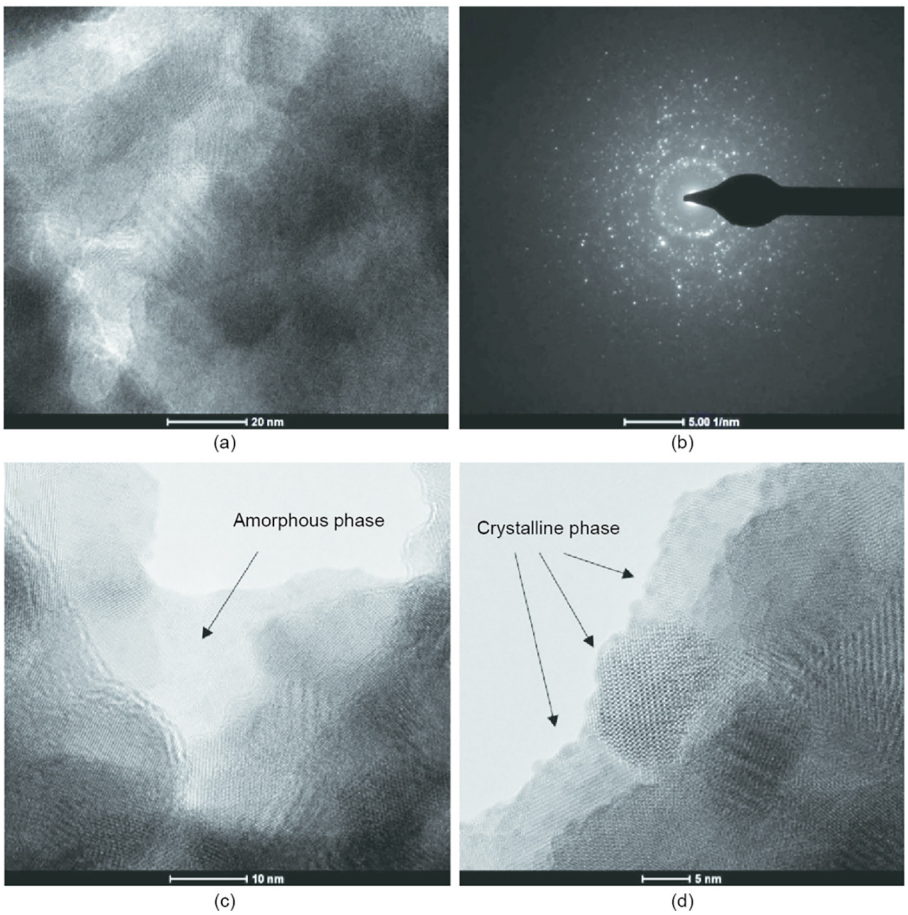

Fig. 7. (a) BF-TEM image (15 min milling time) showing the grain boundaries and nanocrystallites; (b) corresponding SAED pattern of the powder after 15 min of milling time; (c) BF-TEM image of the powdered sample with some degree of amorphization of the surface after 60 min of milling time; (d) BF-TEM image of the surface of the powdered sample with high amount of crystalline phases after 60 min of milling time.

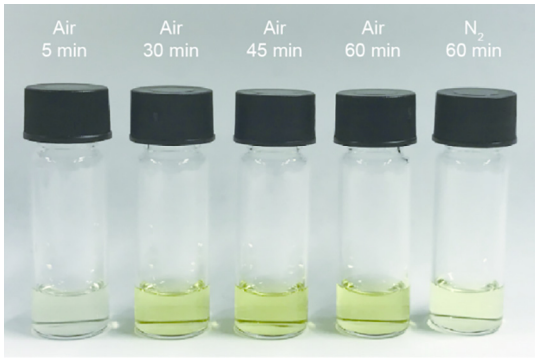

Fig. 8. Color of the leachate when the milling time of LAP lamp phosphor powder, leached in 2 mol·L^{-1} H_2SO_4 at 25 °C and constant L:S ratio of 20 mL·g^{-1}, was increased from left to right. The yellowish color is characteristic of the presence of Ce(IV). The final sample represents the milled sample for 60 min in N_2 atmosphere.

Table 1
Amount of oxidation of Ce(III) (%) as a function of milling time and atmosphere.

Milling time (min)	Atmosphere	Y_{ox} (%)
5	Air	0.2
15	Air	2.2
30	Air	14.4
45	Air	14.7
60	Air	15.0
60	N_2	2.0

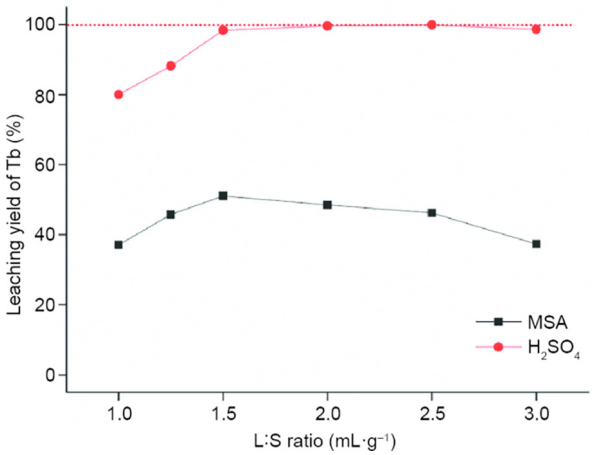

Fig. 9. Changes in the leaching yield of Tb (by concentrated MSA and concentrated H_2SO_4) of simultaneously milled (60 min) LAP lamp phosphor powder using different L:S ratios. MA conditions: 600 r·min^{-1}, ϕ_{ball} = 1 mm, B:P = 50:1.

effects on the leaching yield, while leaching of the wet-milled sample had little effect. This finding suggests that the increase in surface area and the decrease in particle size of the finely ground particles are not the major factors influencing the rate of leaching. During the wet-milling mode, aggregate formation can be avoided due to the wetting of the particles, resulting in very fine nanoparticles. However, the liquid also causes damping of the mechanical forces, thus reducing the physicochemical effects. During the

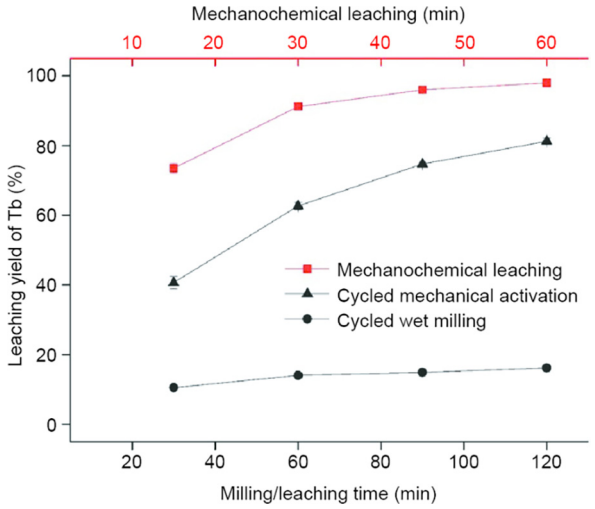

Fig. 10. Changes in the leaching yield of REEs of mechanochemical, cycled mechanically activated, and cycled wet-milled LAP lamp phosphor powder. MA conditions: 600 r·min^{-1}, ϕ_{ball} = 1 mm, B:P = 50:1. Error bars indicate standard deviations, which are calculated based on the leaching results from three replicates. Error bars that are not visible are smaller than the symbol of the data point.

mechanochemical leaching mode, the changes in crystallite size, lattice, and strain will therefore also be reduced. It is postulated that within this mode, the physicochemical changes occur at the outer shell of the particle, creating more reactive sites. These sites react with the acid that is present in the vessel, forming rare-earth sulfates. In addition, a number of highly excited, short-lived states may form (e.g., lattice vibration, fresh surface), which are only present when milling is combined with simultaneous leaching (i.e., reactive milling). If MA and chemical leaching are integrated into a single common stage, all excitation states can be used to our benefit. Therefore, this method has both operational and economic benefits due to equipment downsizing and drastic reduction of the operation time.

4. Conclusions

MC is an established technique for the recovery of critical metals from waste streams. The results indicate that both MA and mechanochemical leaching have a positive influence on the acidic leaching of REEs from LAP in lamp phosphor waste. The recovery of REEs increased 200 times as a result of MA before leaching in a 2 mol·L^{-1} H_2SO_4 solution, compared with the leaching of non-activated material. Due to the formation of a polycrystalline material—and not an amorphous material, as is commonly argued—creating grain boundaries that include crystal defects, the breaking of existing bonds is facilitated. This expedites mass transfer in the solids, thus improving the leaching yield. A comparison of cycled mechanically activated and solvo-mechanochemical leaching of LAP showed that the combined mechanochemical leaching was profoundly more effective. By introducing a cycled MA mode, activated powder can be removed and cycled in a second activation loop, thus improving the overall REE recovery of the process. A solvo-mechanochemical method consisting of an integrated leaching and MA step was developed, which permitted up to 98% recovery of REEs at room temperature using low amounts of concentrated H_2SO_4 as lixiviant. The solvo-mechanochemical method not only resulted in a higher leaching yield in comparison with a cycled MA method, but also reduced the required time by six-fold. The proposed solvo-mechanochemical method is, therefore, an efficient and simple process that reduces the time and energy requirement, and also reduces both acid consumption and wastewater production.

Acknowledgements

This research is supported by KU Leuven (GOA/13/008 and IOF-KP RARE^3). Steff Van Loy thanks FWO-Flanders for a SB PhD fellowship (1S23518N). Koen Binnemans acknowledges the European Research Council (ERC) under the European Union's Horizon2020 Research and Innovation Programme: Grant Agreement 694078—Solvometallurgy for critical metals (SOLCRIMET). The authors would like to extend their gratitude to Alexander Neirinckx and the Electron Microscopy for Materials Science Research Group (EMAT, University of Antwerp) for their support in the HR-TEM imaging.

Compliance with ethics guidelines

Steff Van Loy, Koen Binnemans, and Tom Van Gerven declare that they have no conflict of interest or financial conflicts to disclose.

References

[1] Goonan TG. USGS rare earth elements—end use and recyclability. Report. Washington, DC: US Department of the Interior; 2011.
[2] Schüler D, Buchert M, Liu R, Dittrich S, Merz C. Study on rare earths and their recycling. Report. Darmstadt: Öko-Institut eV; 2011. Deutsch.
[3] Dutta T, Kim KH, Uchimiya M, Kwon EE, Jeon BH, Deep A, et al. Global demand for rare earth resources and strategies for green mining. Environ Res 2016;150:182–90.
[4] Binnemans K, Jones PT, Blanpain B, Van Gerven T, Yang Y, Walton A, et al. Recycling of rare earths: a critical review. J Clean Prod 2013;51:1–22.
[5] Binnemans K, Jones PT, Blanpain B, Van Gerven T, Pontikes Y. Towards zero-waste valorisation of rare-earth-containing industrial process residues: a critical review. J Clean Prod 2015;99:17–38.
[6] Pellegrini M, Godlewska L, Millet P, Gislev M, Grasser L. EU potential in the field of rare earth elements and policy actions. In: Proceedings of 2nd Conference on European Rare Earth Resources (ERES 2017); 2017 May 28–31; Santorini, Greece; 2017. p. 12–5.
[7] Binnemans K, Jones PT. Rare earths and the balance problem. J Sustain Metall 2015;1(1):29–38.
[8] Vander Hoogerstraete T, Blanpain B, Van Gerven T, Binnemans K. From NdFeB magnets towards the rare-earth oxides: a recycling process consuming only oxalic acid. RSC Adv 2014;4(109):64099–111.
[9] Onal MAR, Borra CR, Guo M, Blanpain B, Van Gerven T. Recycling of NdFeB magnets using sulfation, selective roasting, and water leaching. J Sustain Metall 2015;1(3):199–215.
[10] Yang X, Zhang J, Fang X. Rare earth element recycling from waste nickel-metal hydride batteries. J Hazard Mater 2014;279:384–8.
[11] Meshram P, Pandey BD, Mankhand TR. Process optimization and kinetics for leaching of rare earth metals from the spent Ni-metal hydride batteries. Waste Manage 2016;51:196–203.
[12] Tunsu C, Petranikova M, Gergorić M, Ekberg C, Retegan T. Reclaiming rare earth elements from end-of-life products: a review of the perspectives for urban mining using hydrometallurgical unit operations. Hydrometallurgy 2015;156:239–58.
[13] Tunsu C, Petranikova M, Ekberg C, Retegan T. A hydrometallurgical process for the recovery of rare earth elements from fluorescent lamp waste fractions. Separ Purif Tech 2016;161:172–86.
[14] Yang Y, Walton A, Sheridan R, Güth K, Gauß R, Gutfleisch O, et al. REE recovery from end-of-life NdFeB permanent magnet scrap: a critical review. J Sustain Metall 2017;3(1):122–49.
[15] Binnemans K, Jones PT. Perspectives for the recovery of rare earths from end-of-life fluorescent lamps. J Rare Earths 2014;32(3):195–200.
[16] Braconnier JJ, Rollat A, inventors. Method for recovering rare-earth elements from a solid mixture containing a halophosphate and a compound of one or more rare-earth elements. United States Patent US 8501124. 2013 Aug 6.
[17] Ippolito M, Innocenzi V, De Michelis I, Medici F, Vegli F. Rare earth elements recovery from fluorescent lamps: a new thermal pretreatment to improve the efficiency of the hydrometallurgical process. J Clean Prod 2017;153:287–98.
[18] Brisson VL, Zhuang WQ, Alvarez-Cohen L. Bioleaching of rare earth elements from monazite sand. Biotechnol Bioeng 2016;113(2):339–48.
[19] Tan Q, Li J. Recycling metals from wastes: a novel application of mechanochemistry. Environ Sci Technol 2015;49(10):5849–61.
[20] Ou Z, Li J, Wang Z. Application of mechanochemistry to metal recovery from second-hand resources: a technical overview. Environ Sci Process Impacts 2015;17(9):1522–30.
[21] Van Loy S, Binnemans K, Van Gerven T. Recycling of rare earths from lamp phosphor waste: enhanced dissolution of $LaPO_4$:Ce^{3+},Tb^{3+} by mechanical activation. J Clean Prod 2017;156:226–34.

[22] Baláž P, Achimovičová M. Mechano-chemical leaching in hydrometallurgy of complex sulphides. Hydrometallurgy 2006;84(1–2):60–8.
[23] Baláž P, Achimovičová M, Baláž M, Billik P, Cherkezova-Zheleva Z, Criado JM, et al. Hallmarks of mechanochemistry: from nanoparticles to technology. Chem Soc Rev 2013;42(18):7571–637.
[24] Tan Q, Deng C, Li J. Innovative application of mechanical activation for rare earth elements recovering: process optimization and mechanism exploration. Sci Rep 2016;6(1):19961.
[25] Tan Q, Deng C, Li J. Enhanced recovery of rare earth elements from waste phosphors by mechanical activation. J Clean Prod 2017;142:2187–91.
[26] Song G, Yuan W, Zhu X, Wang X, Zhang C, Li J, et al. Improvement in rare earth element recovery from waste trichromatic phosphors by mechanical activation. J Clean Prod 2017;151:361–70.
[27] Senna M. How can we make solids more reactive? Basics of mechanochemistry and recent new insights. ChemTexts 2017;3(2):4–13.
[28] Munnings C, Badwal SPS, Fini D. Spontaneous stress-induced oxidation of Ce ions in Gd-doped ceria at room temperature. Ionics (Kiel) 2014;20(8):1117–26.
[29] Um N, Hirato T. A hydrometallurgical method of energy saving type for separation of rare earth elements from rare earth polishing powder wastes with middle fraction of ceria. J Rare Earths 2016;34(5):536–42.
[30] Gernon MD, Wu M, Buszta T, Janney P. Environmental benefits of methanesulfonic acid. Comparative properties and advantages. Green Chem 1999;1(3):127–40.
[31] Binnemans K, Jones PT. Solvometallurgy: an emerging branch of extractive metallurgy. J Sustain Metall 2017;3(3):570–600.